Direct Observation of the Reactivity of Electrons toward Gold Nanoparticles in Aqueous Solution

Zhiwen Jiang, Mehran Mostafavi

NANO LETTERS

pubs.acs.org/NanoLett Letter

Direct Observation of the Reactivity of Electrons toward Gold Nanoparticles in Aqueous Solution

Zhiwen Jiang and Mehran Mostafavi*

Cite This: https://doi.org/10.1021/acs.nanolett.4c03396 Read Online

ACCESS | Metrics & More | Article Recommendations | Supporting Information

ABSTRACT: The catalytic activity of gold nanoparticles (AuNPs) has been widely acknowledged; however, Au NPs are considered to be highly inert as radiosensitizers in biological systems. This apparent discrepancy across different fields complicates the understanding of their interfacial reactivity, particularly in terms of electron transfer reactions. Here, we employ pulse radiolysis to determine the rate constants for the reactions of electrons with AuNPs in aqueous solution. Our investigation of AuNPs with different sizes and surface modifications demonstrates the potential influence of the AuNPs design on electron transfer reactions. These findings address long-standing mechanistic contradictions and underscore the significance of interfacial electron dynamics on AuNPs in both catalytic and biological processes.

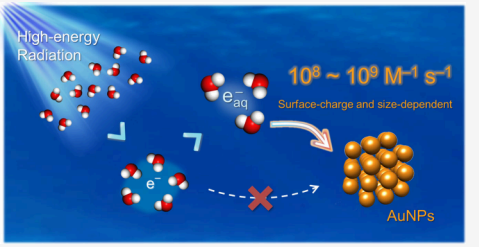

KEYWORDS: *Electron transfer reaction, gold nanoparticles, interfacial dynamics, transient kinetics, pulse radiolysis*

Gold nanoparticles (AuNPs) have been accentuated in life sciences over the past decades and continue to exhibit escalating prominence.[1−3] AuNPs, which feature a large surface area, are relatively easy to synthesize, shape, and functionalize. Most notably, they are considered to be chemically stable. These nanoparticles, typically ranging in size from ten to one hundred nanometers, also exhibit strong cellular penetration. Extensive research has explored the multifaceted applications of AuNPs in cancer therapy, employing ionizing radiation, phototherapy, and combined therapeutic and diagnostic approaches.[4−6] AuNPs have heralded transformative potential in radiotherapy by augmenting the therapeutic efficacy of ionizing radiation while concurrently mitigating associated side effects, as demonstrated in both in vitro and in vivo studies.[7,8] This pivotal role is frequently attributed to their capacity to enhance dose absorption due to their high atomic number (Z), which leverages physical mechanisms and elicits the emission of secondary electrons and X-rays.[9−11] Consequently, AuNPs are traditionally regarded solely as vectors with no intrinsic chemical activity.

However, recent studies have shown that AuNPs do not merely act as passive vectors; they can also play a catalytic role in solutions even at room temperature and alter reaction mechanisms within a given environment.[12−15] Quantitative results obtained in the catalysis of alcohol radical oxidation and the hydroxylation of acetanilide demonstrate that AuNPs can significantly change the reaction pathways of transient species induced by high-energy radiation.[16−18] For example, in the presence of O_2, a 40-fold decrease in the formation of the acetanilide hydroxylation product is observed.[16] This finding is unexpected, as oxygen typically stimulates hydroxylation reactions in the absence of AuNPs. Additionally, it has been highlighted that AuNPs can catalyze electron transfer from a donor to an acceptor, potentially altering the balance of oxidative stress in a given environment.[17−19] Despite these insights, there are still several gaps in the literature regarding the reactivity of AuNPs in solution under irradiation. Key questions remain, such as the reactivity of AuNPs toward the solvated electrons or even presolvated electrons, the rate constant of these reactions, and the subsequent fate of the nanoparticles.

An ultrafast presolvated electron capture in aqueous solutions of room-temperature ionic liquid (RTIL) surface-stabilized gold nanoparticles has been reported,[20] with a rate constant of approximately 5×10^{14} M^{-1} s^{-1}. This electron capture is announced to compete with electron solvation and electron-cation recombination reactions. However, these measurements were performed indirectly using muon spectroscopy, and the concentration of the nanoparticles was used to estimate the rate constant. Later, direct observations via pulse radiolysis suggested the capture of presolvated electrons by AuNPs.[21] This study did not consider the potential reactivity of the AuNP stabilizer with the electrons. Recently, pulse radiolysis measurements of aqueous solution containing AuNPs showed no increase in secondary electrons under a 7 ps electron pulse ionization, indicating the absence of higher primary radical production in the presence of AuNPs.[22] These results decisively established that AuNPs do not instigate a

Received: July 16, 2024
Revised: September 11, 2024
Accepted: September 16, 2024

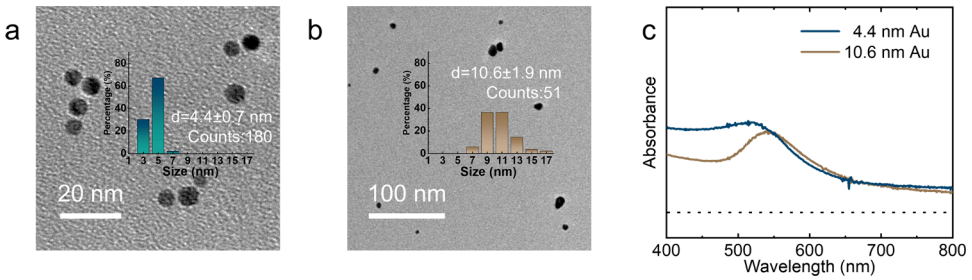

Figure 1. TEM images of Au NPs with the size of 4.4 nm (a) and 10.6 nm (b), inset: corresponding size histograms; (c) UV−vis absorption spectra of Au NPs.

heightened generation of primary water radicals at concentrations similar to those used in biomedical applications and radiation contexts. Additionally, no measurable increase in solvated electron formation was observed, and AuNPs did not scavenge the presolvated electron. The decay of the hydrated electron produced with a high dose per pulse (ca. 100 Gy/pulse) remained unaffected in the presence of AuNPs within 1 μs.

More recently, we investigated the reactivity of $CO_2^{\bullet-}$ radical with AuNPs.[23] $CO_2^{\bullet-}$ is a potent electron donor radical in an aqueous solution. It was found that the $CO_2^{\bullet-}$ radical can bond to the surface of AuNPs for at least 1 ms, which is 100 times longer than the lifetime of bulk $CO_2^{\bullet-}$ in the absence of AuNPs. Given that solvated and presolvated electrons are produced under irradiation in aqueous solution and bioenvironment conditions, here we conducted pulse radiolysis measurements of AuNPs solutions. These experiments were designed to observe directly the kinetics of the hydrated electron to comprehensively address the question of the reactivity of the electrons with AuNPs by the selection of appropriate experimental conditions.

To elucidate the reactivity of AuNPs, we synthesized two different sizes of AuNPs by a chemical reduction method (details in the SI). The size of AuNPs was controlled by adjusting the radio of Au^{3+}/BH_4^-, without the addition of any surfactants, to prevent potential side reactions between the surfactant and electrons.[24] Transmission electron microscopy (TEM) images revealed synthesized AuNPs with narrow size distribution at 4.4 and 10.6 nm, respectively (Figure 1a-b). In the UV−vis spectra (Figure 1c), the 10.6 nm AuNPs exhibited a strong surface plasmon resonance (SPR) band centered at 540 nm. The SPR band of smaller AuNPs (4.4 nm) shifted to the blue (λ = 520 nm) and evolved into a broad band. These characterizations demonstrate the efficient synthesis of stable AuNPs of two different sizes, 4.4 and 10.6 nm.

Pulse radiolysis is employed to directly determine the quantity of water radical products within 7 ps. According to our previous report,[22] 3 mM AuNPs neither instigate a heightened generation of presolvated electrons (e_{pre}^-) nor react with e_{pre}^- and hydrated electrons (e_{aq}^-). For the present work, the initial intensity of the transient absorption at 700 nm displays no noticeable change in the absence or presence of AuNPs. This result confirms that AuNPs do not react with e_{pre}^-, as previously observed (Figure 2a-b). Regarding the reactivity of AuNPs toward e_{aq}^-, we reduced the dose per pulse to ca. 10 Gy/pulse to prevent the dominance of competitive recombination reaction ($e_{aq}^- + e_{aq}^- \rightarrow OH^- + H_2$ $k_1 = 6.0 \times 10^9$ M^{-1} s^{-1})[25] caused by an excessive concentration of e_{aq}^-. The competitive reaction between e_{aq}^- and H^+ ($e_{aq}^- + H^+ \rightarrow H^\bullet$ $k_2 = 2.4 \times 10^{10}$ M^{-1} s^{-1})[26] was also suppressed by adjusting

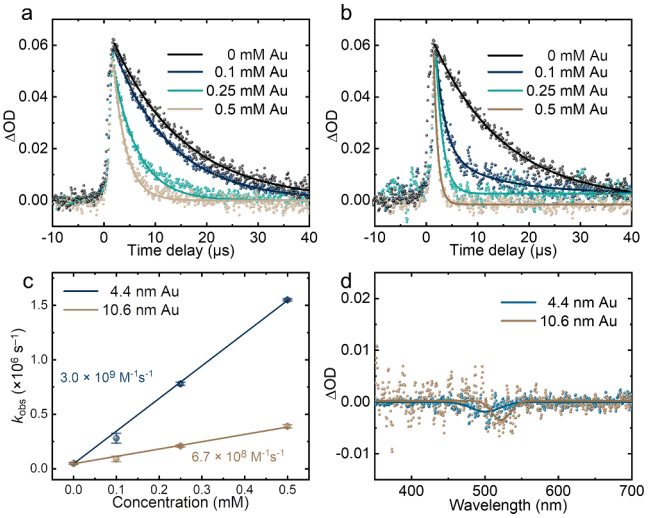

Figure 2. Pulse radiolysis measurement in Ar-saturated alkaline aqueous solutions (pH 12) containing 0.1 M tert-butanol: Transient absorption kinetic traces of e_{aq}^- at 700 nm with different concentrations of 10.6 nm (a) and 4.4 nm (b) Au NPs (ca. 10 Gy/pulse); (c) Apparent e_{aq}^- decay rate as a function of the concentration of Au NPs from (a) and (b). (d) Transient absorption spectrum at 40 μs corresponding to the bleaching of the plasma band of Au NPs.

the pH to 12 (Figure S1). Under these optimized conditions, the transient kinetics of e_{aq}^- remains stable within 1 μs under 6 Gy/pulse, in stark contrast to the decay under 120 Gy/pulse. With the pH 12 condition, the lifetime of e_{aq}^- is drastically increased, which provided a prerequisite for observing the reaction between AuNPs and e_{aq}^-.

To exclude the side reaction between any residence and e_{aq}^-, the supernatant of the AuNPs solution was assigned to the 0 mM sample. As shown in Figure 2a, in the absence of AuNPs, the decay of e_{aq}^- in contrast to the previous work was prolonged to approximately 40 μs due to the lower dose per pulse. With increasing AuNPs concentration, e_{aq}^- presented accelerated decay, and the second-order constant was determined to be 6.7×10^8 M^{-1} s^{-1} (Figure 2c). Moreover, smaller AuNPs (4.4 nm) also suggested similar transient kinetics with a rate constant of 3.0×10^9 M^{-1} s^{-1} (Figure 2b,c). These values are reported by the atomic concentrations of AuNPs.

In addition to decaying e_{aq}^-, the electron transfer also alters the plasma frequency of AuNPs, causing a blueshift in their SPR band.[27,28] This blueshift results in the bleaching of the SPR band in the absorption spectrum (Figure 2d), which enables us to detect the electron transfer and to quantify electron concentration in real-time. As shown in Figure S2, the

https://doi.org/10.1021/acs.nanolett.4c03396
Nano Lett. XXXX, XXX, XXX−XXX

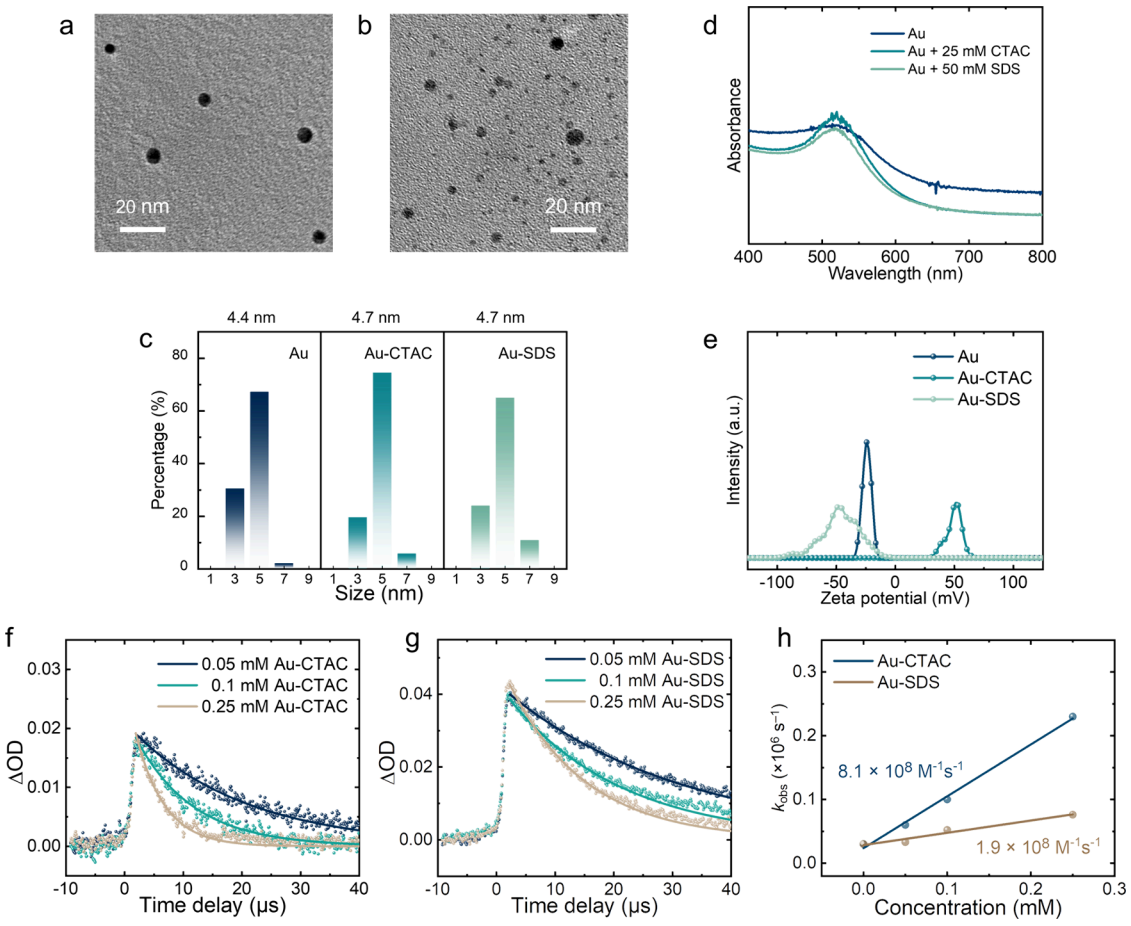

Figure 3. TEM images of Au NPs in 25 mM CTAC (a) or 50 mM SDS (b) solutions, and their size histograms (c) (50 nanoparticles measured); UV−vis spectra (d) and zeta potential (e) of Au NPs. Transient absorption kinetic traces of e_{aq}^- at 700 nm with different concentrations of Au NPs in the 25 mM CTAC (f) or 50 mM SDS (g) solutions; (h) Apparent e_{aq}^- decay rate as a function of the concentration of Au NPs from (f) and (g).

time scale of the observed bleaching agrees with the decay of the hydrated electron. The bleaching of the SPR band at 40 μs illustrated the electron transfer from e_{aq}^- to the surface of AuNPs and the electron decay completely. The steady-state absorption spectra reveal a shift in the SPR band from 520 to 515 nm (Figure S3). The relationship between the wavelength shift to the transferred electron density is given by[27]

$$\frac{\Delta N}{2N} = \frac{\Delta\lambda}{\lambda_0}$$

Here, N is the electron density of the metal, and λ_0 is the bulk SPR wavelength. ΔN and $\Delta\lambda_0$ are the change in the nanoparticle electron density and the SPR wavelength shift, respectively. Based on this relationship and the concentration of AuNPs (0.5 mM), the blue-shift indicates a 2% increase in electron density, equivalent to 10 μM electrons. This value is in line with the dose per pulse in our pulse radiolysis experiments.

According to a previous study,[20] the electron capture rate of AuNPs was determined using particle concentration to be 5×10^{14} M^{-1} s^{-1} by muon spectroscopy. These findings have led to divergent mechanistic understandings of the reactivity of AuNPs with electrons. Steady-state muon spectroscopy cannot provide the transient kinetics of e_{pre}^- or e_{aq}^- to directly prove that the reaction occurred. More importantly, it is crucial to investigate the reaction between AuNPs and electrons through interfacial dynamics. We cannot directly substitute the concentration of AuNPs since every AuNPs involves many active sites for reactions. The rate constants we determined well corroborate this issue. When the size of AuNPs decreases from 10.6 to 4.4 nm, the concentration of AuNPs increases by the cube of the radius, ca. 14.8 times. If we were to simply substitute the value, the rate constant should increase by the same factor. However, it is actually much lower, only 4.5 times. In fact, if AuNPs concentrations were substituted in this work, the reaction rates would be estimated to be 1.6 and 5.2×10^{16} M^{-1} s^{-1}. This value aligns with previous result but contradicts the identical yield of e_{pre}^- in the absence and presence of AuNPs.[20] Therefore, we propose expressing the rate constant in terms of the concentration of Au atoms. Alternatively, we consider the exposed Au atoms on the surface of AuNPs as active sites. The proportions of these Au atoms are calculated to be approximately 27.8% for 4.4 nm AuNPs and 11.5% for 10.6 nm AuNPs, respectively. The corresponding rate constants can be estimated to be 1.1×10^{10} M^{-1} s^{-1} for 4.4 nm AuNPs and 5.8×10^9 M^{-1} s^{-1} for 10.6 nm AuNPs, which is much slower than the solvation of electrons. These rate constants are almost completely controlled by diffusion. To the best of our knowledge, this observation represents the first report of the reaction between AuNPs and e_{aq}^- from a direct time-resolved prospective.

Given the limitations of bulk AuNPs, such as challenges in stable dispersion for catalytic applications and in vivo delivery in the radiobiology domain, AuNPs are often surface-modified

https://doi.org/10.1021/acs.nanolett.4c03396
Nano Lett. XXXX, XXX, XXX−XXX

with surfactants.[29−31] These modifications can optimize key desired features for various functions but may impact the interfacial reaction kinetics due to the altered charge environment.[24] To gain deeper insights into the interfacial electron transfer reaction under different charge conditions, we modified the synthesized AuNPs by adding typical surfactants, CTAC and SDS. Although the SPR band became narrower and shifted slightly to 518 nm, TEM images and the corresponding size histograms confirmed that the modification induced negligible influence on the size and stability of the obtained AuNPs (Figure 3a-d). The AuNPs enlarged slightly from 4.4 to 4.7 nm without significant aggregation. Zeta potential measurements confirmed the different charge modifications of Au-CTAC and Au-SDS, with values of ca. −49.3 and 50.3 mV, respectively (Figure 3e).

The transient kinetics at 700 nm exhibit a similar decay of e_{aq}^- in the presence of Au-CTAC (Figure 3f). The second-order rate constant of e_{aq}^- with Au-CTAC was determined to be 8.1×10^8 M^{-1} s^{-1} (Figure 3h), which is 73% lower than that for bulk 4.4 nm AuNPs. In stark contrast, Au-SDS shows a more severely retarded decay of e_{aq}^-, with the decay not completing within 40 μs (Figure 3g). The rate constant decreased to 1.9×10^8 M^{-1} s^{-1}, an order of magnitude lower than that of unmodified AuNPs. These reduced rates demonstrate that the modified AuNPs are still capable of scavenging e_{aq}^-. However, both positive and negative charge modifications hinder the reaction between e_{aq}^- and AuNPs. Since of the electrostatic interaction between the negative charges and e_{aq}^-, the negative charge modification of AuNPs more effectively hampers the migration of e_{aq}^- around the AuNPs at the same level of zeta potential, leading to lower reaction rates. The reduced second-order rate constants for e_{aq}^- with both Au-CTAC and Au-SDS demonstrate the critical role of surface modifications in modulating the reactivity of AuNPs (Table 1). Our results highlight the importance of considering surface modifications in designing AuNP-based systems for specific applications. According to these results, it is worth noting that the surface charge states of nanoparticles may also regulate the transient kinetics of e_{aq}^-. The rate constant obtained in our pulse experiments may also be influenced by the accumulation of e_{aq}^- on gold nanoparticles, which alters the surface charge. Given that the charge proportion is low (2%, as shown in Figure S3), variation in these rate constants is negligible.

Table 1. Rate Constants for the Reactions of Hydrated Electron with Different Types of AuNPs

Zeta potential (mV)	Size (nm)	k (M^{-1} s^{-1}) from atomic concentration	k (M^{-1} s^{-1}) from nanoparticle concentration
−24.1 (without surfactant)	4.4	3.0×10^9	1.6×10^{16}
	10.6	6.7×10^8	5.2×10^{16}
−49.3 (with 25 mM CTAC)	4.7	8.1×10^8	5.2×10^{15}
−50.3 (with 50 mM SDS)	4.7	1.9×10^8	1.2×10^{15}

In summary, the controversial reactivity of AuNPs toward e_{pre}^- and e_{aq}^- is addressed through direct time-resolved observations. Transient kinetics under low dose rates and alkaline conditions provide an accurate understanding of their interfacial dynamics and rate constants. The determined rate constants (6.7×10^8 M^{-1} s^{-1} for 10.6 nm AuNPs and 3.0×10^9 M^{-1} s^{-1} for 4.4 nm AuNPs) rule out the reactivity of AuNPs toward e_{pre}^- and verify their high reactivity toward e_{aq}^-. Furthermore, our work highlights the significance of size control and surface modifications in modulating the reactivity of the AuNPs. These insights could pave the way for the more precise engineering of AuNPs with tailored properties for enhanced performance in both catalytic and biomedical applications.

■ ASSOCIATED CONTENT

Supporting Information

The Supporting Information is available free of charge at https://pubs.acs.org/doi/10.1021/acs.nanolett.4c03396.

Transient absorption kinetic traces and absorption spectra for the different dose and pH conditions (PDF)

■ AUTHOR INFORMATION

Corresponding Author

Mehran Mostafavi − *Institute de Chimie Physique, UMR8000 CNRS/Université Paris-Saclay, Orsay 91405, France;* orcid.org/0000-0002-4510-8272; Email: mehran.mostafavi@universite-paris-saclay.fr

Author

Zhiwen Jiang − *Institute de Chimie Physique, UMR8000 CNRS/Université Paris-Saclay, Orsay 91405, France;* orcid.org/0000-0003-3576-2534

Complete contact information is available at: https://pubs.acs.org/10.1021/acs.nanolett.4c03396

Author Contributions

All authors conceived of the work, designed and performed the experiments, analyzed the data, wrote the manuscript, and deeply revised it.

Funding

This work was supported by the Postdoctoral Fellowship Program of CPSF (GZC20232529).

Notes

The authors declare no competing financial interest.

■ ACKNOWLEDGMENTS

We thank Jean-Philippe Larbre for his help during the experiments at ELYSE.

■ REFERENCES

(1) Haume, K.; Rosa, S.; Grellet, S.; Śmiałek, M. A.; Butterworth, K. T.; Solov'yov, A. V.; Prise, K. M.; Golding, J.; Mason, N. J. Gold nanoparticles for cancer radiotherapy: a review. *Cancer Nanotechnol* **2016**, *7*, 1−20.

(2) Guo, T. Physical, chemical and biological enhancement in X-ray nanochemistry. *Phys. Chem. Chem. Phys.* **2019**, *21*, 15917−15931.

(3) Eun Chul, C.; Zhang, Q.; Xia, Y. The effect of sedimentation and diffusion on cellular uptake of gold nanoparticles. *Nat. Nanotechnol.* **2011**, *6*, 385−391.

(4) Elahia, N.; Kamalia, M.; Baghersa, M. H. Recent biomedical applications of gold nanoparticles. *A review Talanta, 2018* **2018**, *184*, 537−556.

(5) Chen, J.; Gong, M.; Fan, Y.; Feng, J.; Han, L.; Xin, H. L.; Cao, M.; Zhang, Q.; Zhang, D.; Lei, D.; Yin, Y. Collective plasmon coupling in gold nanoparticle clusters for highly efficient photothermal therapy. *ACS Nano* **2022**, *16* (1), 910−920.

(6) Murphy, C. J.; Gole, A. M.; Stone, J. W.; Sisco, P. N.; Alkilany, A. M.; Goldsmith, E. C.; Baxter, S. C. Gold nanoparticles in biology: beyond toxicity to cellular imaging. *Acc. Chem. Res.* **2008**, *41* (12), 1721−1730.
(7) Antosh, M. P.; Wijesinghe, D. D.; Shrestha, S.; Lanou, R.; Huang, Y. H.; Hasselbacher, T.; Fox, D.; Neretti, N.; Sun, S.; Katenka, N.; Cooper, L. N.; Andreevc, O. A.; Reshetnyak, Y. K. Enhancement of radiation effect on cancer cells by gold-pHLIP. *Proc. Natl. Acad. Sci. U. S. A.* **2015**, *112* (17), 5372−5376.
(8) Lan, G.; Ni, K.; Veroneau, S. S.; Luo, T.; You, E.; Lin, W. Nanoscale metal−organic framework hierarchically combines high-Z components for multifarious radio-enhancement. *J. Am. Chem. Soc.* **2019**, *141* (17), 6859−6863.
(9) Her, S.; Jaffray, D. A.; Allen, C. Gold nanoparticles for applications in cancer radiotherapy: mechanisms and recent advancements. *Adv. Drug. Delivery Rev.* **2017**, *109*, 84−101.
(10) Howard, D.; Sebastian, S.; Le, Q. V. C.; Thierry, B.; Kempson, I. Chemical mechanisms of nanoparticle radiosensitization and radioprotection: a review of structure-function relationships influencing reactive oxygen species. *Int. J. Mol. Sci.* **2020**, *21*, 579.
(11) Cabello, G.; Nwoko, K. C.; Mingarelli, M.; McLaughlin, A. C.; Trembleau, L.; Feldmann, J.; Cuesta, A.; Smith, T. A. D. Physicochemical tools: toward a detailed understanding of the architecture of targeted radiotherapy nanoparticles. *ACS Appl. Bio Mater.* **2018**, *1* (5), 1639−1646.
(12) Ovalle, V. J.; Hsu, Y. S.; Agrawal, N.; Janik, M. J.; Waegele, M. M. Correlating hydration free energy and specific adsorption of alkali metal cations during CO_2 electroreduction on Au. *Nat. Catal.* **2022**, *5* (7), 624−632.
(13) Gentry, N. E.; Kurimoto, A.; Cui, K.; Cleron, J. L.; Xiang, C. M.; Hammes-Schiffer, S.; Mayer, J. M. Hydrogen on colloidal gold nanoparticles. *J. Am. Chem. Soc.* **2024**, *146* (21), 14505−14520.
(14) Sedano Varo, E.; Egeberg Tankard, R.; Kryger-Baggesen, J.; Jinschek, J.; Helveg, S.; Chorkendorff, I.; Damsgaard, C. D.; Kibsgaard, J. Gold nanoparticles for CO_2 electroreduction: an optimum defined by size and shape. *J. Am. Chem. Soc.* **2024**, *146* (3), 2015−2023.
(15) Murdoch, M.; Waterhouse, G. I. N.; Nadeem, M. A.; Metson, J. B.; Keane, M. A.; Howe, R. F.; Llorca, J.; Idriss, H. The effect of gold loading and particle size on photocatalytic hydrogen production from ethanol over Au/TiO_2 nanoparticles. *Nat. Chem.* **2011**, *3* (6), 489−492.
(16) Shcherbakov, V.; Denisov, S. A.; Mostafavi, M. A mechanistic study of gold nanoparticles catalysis of O_2 reduction by ascorbate and hydroethidine, investigating reactive oxygen species reactivity. *RSC Adv.* **2023**, *13*, 8557−8563.
(17) Shcherbakov, V.; Denisov, S. A.; Mostafavi, M. The mechanism of organic radical oxidation catalysed by gold nanoparticles. *Phys. Chem. Chem. Phys.* **2021**, *23*, 26494−26500.
(18) Shcherbakov, V.; Denisov, S. A.; Mostafavi, M. Selective oxidation of transient organic radicals in the presence of gold nanoparticles. *Nanomaterials* **2021**, *11*, 727.
(19) Pan, Y.; Leifert, A.; Ruau, D.; Neuss, S.; Bornemann, J.; Schmid, G.; Brandau, W.; Simon, U.; Jahnen-Dechent, W. Gold nanoparticles of diameter 1.4 nm trigger necrosis by oxidative stress and mitochondrial damage. *Small* **2009**, *5*, 2067−2076.
(20) Ghandi, K.; Findlater, A. D.; Mahimwalla, Z.; MacNeil, C. S.; Awoonor-Williams, E.; Zaharievb, F.; Gordon, M. S. Ultra-fast electron capture by electrosterically-stabilized gold nanoparticles. *Nanoscale* **2015**, *7* (27), 11545−11551.
(21) Ghandi, K.; Wang, F.; Landry, C.; Mostafavi, M. Naked gold nanoparticles and hot electrons in water. *Sci. Rep.* **2018**, *8* (1), 7258.
(22) Shcherbakov, V.; Denisov, S. A.; Mostafavi, M. On the primary water radicals' production in the presence of gold nanoparticles: Electron pulse radiolysis study. *Nanomaterials* **2020**, *10*, 2478.
(23) Jiang, Z.; Clavaguéra, C.; Hu, C.; Denisov, S. A.; Shen, S.; Hu, F.; Ma, J.; Mostafavi, M. Direct time-resolved observation of surface-bound carbon dioxide radical anions on metallic nanocatalysts. *Nat. Commun.* **2023**, *14* (1), 7116.
(24) Lopez-Sanchez, J. A.; Dimitratos, N.; Hammond, C.; Brett, G. L.; Kesavan, L.; White, S.; Miedziak, P.; Tiruvalam, R.; Jenkins, R. L.; Carley, A. F.; Knight, D.; Kiely, C. J.; Hutchings, G. J. Facile removal of stabilizer-ligands from supported gold nanoparticles. *Nat. Chem.* **2011**, *3*, 551−556.
(25) Schmidt, K. H.; Bartels, D. M. Lack of ionic strength effect in the recombination of hydrated electrons: $(e^-)_{aq} + (e^-)_{aq} \rightarrow 2(OH^-) + H_2$. *Chem. Phys.* **1995**, *190* (1), 145−152.
(26) Shiraishi, H.; Sunaryo, G. R.; Ishigure, K. Temperature dependence of equilibrium and rate constants of reactions inducing conversion between hydrated electron and atomic hydrogen. *J. Phys. Chem.* **1994**, *98* (19), 5164−5173.
(27) Mulvaney, P.; Pérez-Juste, J.; Giersig, M.; Liz-Marzán, L. M.; Pecharromán, C. Drastic surface plasmon mode shifts in gold nanorods due to electron charging. *Plasmonics* **2006**, *1*, 61−66.
(28) Novo, C.; Funston, A. M.; Mulvaney, P. Direct observation of chemical reactions on single gold nanocrystals using surface plasmon spectroscopy. *Nat. Nanotechnol.* **2008**, *3* (10), 598−602.
(29) Wong, C.; Stylianopoulos, T.; Cui, J.; Martin, J.; Chauhan, V. P.; Jiang, W.; Popović, Z.; Jain, R. K.; Bawendi, M. G.; Fukumura, D. Multistage nanoparticle delivery system for deep penetration into tumor tissue. *Proc. Natl. Acad. Sci. U. S. A.* **2011**, *108* (6), 2426−2431.
(30) Choi, C. H.; Alabi, C. A.; Webster, P.; Davis, M. E. Mechanism of active targeting in solid tumors with transferrin-containing gold nanoparticles. *Proc. Natl. Acad. Sci. U. S. A.* **2010**, *107* (3), 1235−1240.
(31) Kumar, R.; Korideck, H.; Ngwa, W.; Berbeco, R. I.; Makrigiorgos, G. M.; Sridhar, S. Third generation gold nanoplatform optimized for radiation therapy. *Transl. Cancer Res.* **2013**, *2* (4), 228−239.

https://doi.org/10.1021/acs.nanolett.4c03396
Nano Lett. XXXX, XXX, XXX−XXX